Tuning the Swing Effect by Chemical Functionalization of Zeolitic Imidazolate Frameworks

Tuning the Swing Effect by Chemical Functionalisation of Zeolitic Imidazolate Frameworks

Claire L. Hobday[a*]†, Thomas D. Bennett[b], David Fairen-Jimenez[c], Alexander J. Graham[a], Carole A. Morrison[a], David. R. Allan[d], Tina Düren[e] and Stephen A. Moggach[a]

a. EaStChem School of Chemistry and Centre for Science at Extreme Conditions, University of Edinburgh, David Brewster Road, Joseph Black Building, Edinburgh EH9 3FJ, UK

b. Department of Materials Science and Metallurgy, University of Cambridge, CB3 0DZ, UK

c. Department of Chemical Engineering & Biotechnology, University of Cambridge, CB2 3RA Cambridge, UK

d. Diamond Light Source, Harwell Campus, Didcot, OX11 ODE, UK

e. Centre for Advanced Separations Engineering, Department of Chemical Engineering, University of Bath, Bath, BA2 7AY, UK

KEYWORDS Metal-organic frameworks; adsorption; porous materials; high-pressure crystallography; molecular simulation; density functional theory

Supporting Information Placeholder

ABSTRACT: (Many zeolitic imidazolate frameworks (ZIFs) are promising candidates for use in separation technologies. Comprising large cavities interconnected by small windows they can be used, at least in principle, as molecular sieves where molecules smaller than the window size are able to diffuse into the material while larger are rejected. However, "swing effect" or "gate opening" phenomena resulting in an enlargement of the windows have proven to be detrimental. Here, we present the first systematic experimental and computational study of the effect of chemical functionalisation of the imidazole linker on the framework dynamics. Using high-pressure (HP) single-crystal X-ray diffraction, density functional theory, and grand canonical Monte Carlo simulations, we show that in the isostructural ZIF-8, ZIF-90 and ZIF-65 functional groups of increasing polarity (-CH_3,-CHO, -NO_2) on the imidazole linkers provide control over the degree of rotation and thus the critical window diameter. On application of pressure, the substituted imidazolate rings rotate resulting in an increase in both pore volume and content. Our results show that the interplay between the guest molecules and the chemical function of the imidazole linker is essential for directing the swing effect in ZIF frameworks and therefore the adsorption performance.

Introduction

Zeolitic imidazolate frameworks (ZIFs) are a class of chemically stable and commercial porous materials.[1,4] Their structures are based on zeolite topologies, where imidazolate (Im, $C_3H_3N_2^-$) and Zn^{2+}, Co^{2+}, Li^+ or B^{3+} ions replace the oxygen and Al^{3+}/Si^{4+} species found in zeolites. Incorporating the Im linker increases the pore sizes compared to zeolites. The ZIF family contains over 100 frameworks which adopt zeolite topologies such as rho (ZIF-11), dft (ZIF-3) and cag (ZIF-4). These different topologies are made possible through functionalisation of the imidazole linker, which results in a change in pore size and surface chemistry.[5] This has led to a plethora of applications of ZIFs in catalysis, drug delivery and gas storage.[6,7] In order to fully exploit the potential of ZIFs it is necessary to fully understand the structural changes of the framework upon guest uptake and the resulting mechanical properties. There has been little work on the mechanical response for example. ZIF-4 ($Zn(Im)_2$, Im = imidazolate) is known to desolvate to a dense form[8] and ZIF-11 ($Zn(bIm)_2$, bIm = benzimidazolate) has been studied to understand how solvent plays a role in stabilising the structure against mechnical stress in ball-milling.[9]

One of the ZIFs that has been widely studied is ZIF-8, ($Zn(mIm)_2$, mIm = 2-methylimidazolate), which crystallises in the cubic space group *I*-43*m* (a=16.9856(16) Å, V=4900.5(8) Å^3) and adopts the sodalite topology (**Fig. 1a**).[4] At ambient pressure and temperature, ZIF-8 contains one central nano-sized pore per unit cell, with a volume of ~2500 Å^3 and pore diameter of 11.6 Å. Connecting these large nanopores are eight six-membered ring (6MR) windows ca. 3.0 Å in diameter and six smaller four-membered ring (4MR) windows of ca. 0.8 Å (**Fig. 1a, Table 1**). Multiple studies have made use of these critically narrow 6MR windows for gas separation in e.g. membranes.[10-13] However, H_2/CH_4 separation experiments (with kinetic diameters of 2.85 Å and 3.80 Å, respectively) illustrated that many molecules with kinetic diameters larger

than the 6MR window, e.g. O_2, N_2 and CH_4, permeate through the structure.[14]

Figure 1: (a) Unit cell of ZIF-8, (b) The angle, θ, represented as the angle that the 100 hkl plane makes with the imidazole linker of the four membered window (c) Unit cell of ZIF-90 and (d) Unit cell of ZIF-65. Zn tetrahedra – cyan, C – black, N – blue, O – red. Note the more closed 4MR of ZIF-65 compared to ZIF-8 and ZIF-90. H-atoms in all structures and the disorder of the CHO function group in ZIF-90 have been removed for clarity.

A structural explanation was later provided by Moggach *et al.*, who reported a pressure-induced phase transition in diamond anvil cell experiments using a 4:1 methanol:ethanol hydrostatic medium. Initial cell volume expansion (for pressures up to 0.18 GPa) from

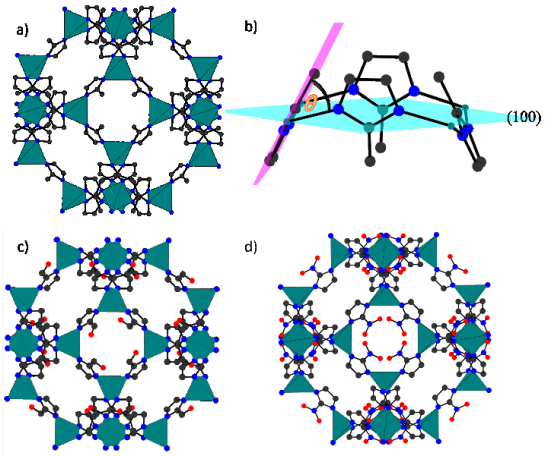

penetration of the hydrostatic medium into the pores was followed by compression at 0.90 GPa.[1] At 1.47 GPa, a single-crystal to single-crystal phase transition took place to a previously unobserved phase (referred to as ZIF-8-HP), involving rotation of the mIm linker. The angle of rotation, ***θ***, defined as the angle between the (100) plane and the mean plane passing through the mIm ring increased from 64.3° at ambient pressure to 89.7° at 1.47 GPa **(Fig. 1b)**. This rotation resulted in an increase in the diameter of the 4MR and 6MR windows from 0.8 Å to 2.2 Å, and 3.0 Å to 3.6 Å, allowing more MeOH and EtOH molecules to enter the framework.[1] Using a combination of grand canonical Monte Carlo (GCMC) simulations and in situ powder X-ray diffraction (PXRD), Fairen-Jimenez *et al* later demonstrated that the same phase transition took place upon gas adsorption at much lower pressure (for N_2 at 77 K it can be observed at ~0.02 bar)[15,16] due to the adsorption of additional molecules in the 4MR windows. Zhang et al showed that this phenomenon is dependent on the ZIF-8 particle size.[17] In addition, the vibrational mode linked to the gate opening has been observed in the terahertz region (< 50 cm^{-1}) and increase in pore volume and content compared to ZIF-8HP (~300 Å3 and 1087 e-/uc compared to 100 Å3 and ~636 e-/uc). predicted by ab initio density functional simulations.[2,18] The effect of hydrostatic media on the compression of ZIF-8 has also been studied demonstrating that the framework has different compressibilites in different media.[19]

Replacement of the -CH_3 substituent on the mIm linker with either -CHO or -NO_2 groups leads to the isostructural and isosymmetric ZIF-90 $(Zn(ICA))_2$, ICA = imidazolate-2-carboxyaldehyde) and ZIF-65 $(Zn(nIm)_2$, nIm = 2-nitroimidazolate), respectively (**Fig. 1c and 1d**). The chemical functionalisation result in different linker orientation and therefore different values for *θ* and the 4MR and 6MR diameters (**Table 1**). These functionalities give the opportunity to tune the host-guest interactions which has been, for example, demonstrated for CO_2 adsorption where post-synthetic modification of ZIF-90 enhanced H_2 selectivity over CO_2[20] and ZIF-65 displays an increased affinity for CO_2,[21,22] compared to ZIF-8 due to the NO_2 functionality.

Results and Discussion

However, the influence of the functionality on the framework dynamics and mechanical properties has not been systematically studied. Here, we present a combined high-pressure (HP) single-crystal diffraction and computational study on three isostructural ZIFs: ZIF-8, ZIF-90 and ZIF-65 in order to understand the effect of imidazole functionality and guest molecule uptake on swing effect behaviour.

Table 1: Diameter of 4MR and 6MR windows in ZIF-8, ZIF-65 and ZIF-90

ZIF	*Lattice parameter /Å*	*Pore volume /Å³*	*θ / °*	*4MR diameter / Å*	*6MR diameter /Å*
ZIF-8	16.9856(16)	2500	64.3	0.8	3.0
ZIF-90	17.0758(13)	2354	66.5	1.4	3.2
ZIF-65	17.3185(2)	2619	46.3	0.8	3.2

All diameters calculated in Mercury, with 0.2 Å grid spacing.[2]

Following X-ray data collection at ambient temperature and pressure, single-crystals of both ZIF-90 and ZIF-65 were placed in modified Merrill-basset diamond anvil cells (DACs), [23,24] along with ruby chips (for pressure calibration)[25] and surrounded by methanol:ethanol (4:1) mixture (SI-1 for experimental details).[1,26]

For ZIF-90, on increasing pressure to 0.34 GPa, the unit cell volume increased by 3.40%, resulting in an increase in pore size of 300 Å³ **(Fig. 2)**. A small decrease in *θ* of 9.3° coincided with a decrease in electron density in the pores from 981 to 238 e^-/uc (**Fig. S2).** Upon increasing pressure further to 0.88 GPa, the unit cell compressed by 0.37% and *θ* increased from 21.3° to 78.6°. At this stage, transformation to a HP phase similar to that of ZIF-8-HP (hereafter referred to as ZIF-90-HP), was observed. *θ* continued increasing to 84.1° at 1.95 GPa, where the pore volume and content reached a maximum, measuring 2612 Å³ and 1087 e^-/uc respectively (**Fig. S2**). The behavioural trends in *θ* and pore volume are similar to that for ZIF-8 reported previously, where a jump in *θ* from 59.7° to 89.7° between 0.96 GPa and 1.47 GPa corresponds to the gate-opening transition to ZIF-8HP.[1] The maximum value of *θ* for ZIF-90HP at 1.96 GPa was therefore slightly less than that of ZIF-8HP at 1.47 GPa, though the larger 4MR window (**Table 2**) of ZIF-90-HP explains the increase in pore volume and content compared to ZIF-8HP (~300 Å³ and 1087 e^-/uc compared to 100 Å³ and ~636 e^-/uc).

Turning to ZIF-65, a unit cell volume expansion of 0.70%, and increase in pore void volume of ~50 Å³ at 0.11 GPa indicated hydrostatic media penetration into the pores.[27] In contrast to the decrease in *θ* observed in ZIF-8 and ZIF-90, here *θ* increased from 46.3° to 48.5°. This rotation caused the 4MR window to increase in size from 0.8 to 1.0 Å, while the 6MR window remained unchanged (**Table 2**). Increasing pressure further to 0.73 GPa saw the onset of the ZIF-65-HP phase, which elicited a decrease in both unit cell volume (2%) and *θ* (from 48.6° to 37.3°). This corresponded to a decrease in 4MR diameter from 1.0 to 0.6 Å and an increase in the 6MR diameter from 3.2 to 3.6 Å. Further increases in pressure to 4.77 GPa resulted in negligible changes to *θ* (30.9°) and a linear decrease in void volume. Compression of the unit cell volume was

accompanied by a steady increase in electron density in the pore to 3.10 GPa (from 280 to ~ 540 e^-/uc), whereby a plateau was reached and maintained to 4.77 GPa. This latter pressure marked the highest pressure point for which diffraction data could be collected and solved (**Fig. 3**). Above this pressure, the single crystal fractured and became amorphous. ZIFs are often observed to become amorphous on direct compression, and have been predicted to be rather unstable on applying pressure.[28,29] The inclusion of solvent stabilises ZIF-65 to external pressure, which has been seen in other MOFs such as CuBTC and MOF-5.[27,30]

The structure of ZIF-65-HP does not resemble that of ZIF-8-HP or ZIF-90-HP (**Fig. 3**). Rotation of the organic linkers to smaller values of θ was observed, compared to the latter two high pressure structures which coincided with an increase in θ. Interestingly, the intermolecular N…O distance (where N is contained within one NO_2 headgroup and O within an adjacent NO_2 headgroup (Fig. S3)) across the 4MR decreased by ~0.5 Å (Table S2). The fact that these -NO_2 groups move towards each other suggest that unlike CH_3…CH_3 interactions the interaction between these groups are mildly favourable. This rationale is consistent with the observation that in certain geometries, stacking of NO_2 groups leads to interaction energies comparable to C=O…H-C interactions.[31,32] As a result of these high-pressure geometries, adsorption of guest molecules is improved due to the increased size of channels linking the central nanopore (**Fig. 3**), encouraging percolation of guest molecules between pores.

By using a mixture of 4:1 methanol:ethanol, we used a pressure transmitting medium that is hydrostatic to high-pressures (12 GPa) and can enter the pores of the ZIFs. In order to determine its role in the transformation of the AP to the HP structures, single point energy calculations were undertaken on guest-free ZIF-8, ZIF-90 and ZIF-65 as a function of ligand rotation. To begin with, geometry optimisation of the ambient pressure structures using the periodic CASTEP code (for full details see SI-1) were performed, giving values of θ comparable to the ambient pressure values, measuring 63.4°, 55.5°, 50.2° for ZIF-8, ZIF-90 and ZIF-65 respectively compared to the ambient crystal structure values of 64.3°, 66.5° and 46.5°. Deviation in the latter two cases is ascribed to solvent presence in the pores in the experimental data. θ was then varied (i.e. the Im linkers rotated) by 30°, in 5° increments, in both positive and negative directions relative to the equilibrium structure. Relative energies with respect to the equilibrium structure were calculated and are given in kJ mol^{-1} per imidazolate linker. **Fig. 4** shows the results of the single point energy calculations (see **Table S3** for more information). Relatively flat potential energy surfaces were revealed, indicating that energy penalty to rotate the linkers are very low. For ZIF-8 (which had a starting θ of 64.3°), the energy penalty to the rotation of the mIm linker to the ZIF-8-HP phase (where θ = 89.7°) was relatively small (~8 kJ mol^{-1}). However, the

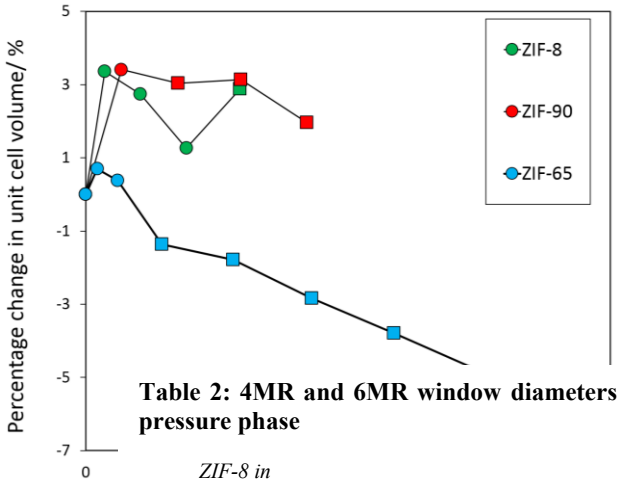

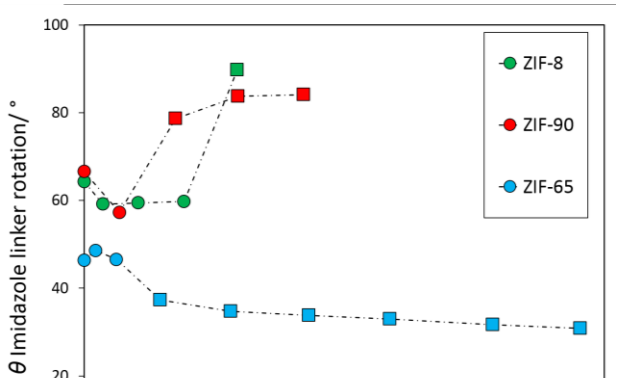

Figure 2: Ev
Where AP a
al.[1]

Table 2: 4MR and 6MR window diameters of ZIF-8, ZIF-65 and ZIF-90 at pressure. * marks the onset to the high-pressure phase

ZIF-8 in MeOH/EtOH	*4MR*	*6MR*	*ZIF-65 in MeOH/EtOH*	*4MR*	*6MR*	*ZIF-90 in MeOH/EtOH*	*4MR*	*6MR*
Pressure / GPa	*diameter / Å³*	*diameter / Å³*	*Pressure / GPa*	*diameter / Å³*	*diameter / Å³*	*Pressure / GPa*	*diameter / Å³*	*diameter / Å³*
0.0	0.8	3.0	0.0	0.8	3.2	0.0	1.4	3.2
0.18	0.6	3.0	0.11	1.0	3.2	0.34	1.0	3.2
0.52	0.6	3.0	0.30	1.0	3.2	0.88*	2.4	3.4
0.96	0.6	3.0	0.73*	0.6	3.6	1.47*	2.6	3.6
1.47*	2.2	3.6	1.40*	0.6	3.6	1.95*	2.4	3.6
			2.15*	0.4	3.6			
			2.94*	0.4	3.8			
			3.93*	0.4	3.8			
			4.77*	0.4	3.8			

same rotation by 25° in the opposite direction had a much larger energy penalty, equating to ~160 kJ mol^{-1}. Due to steric hindrance

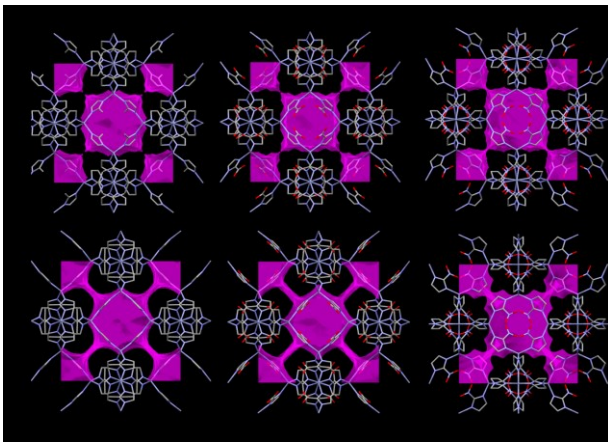

Figure 3: Capped stick diagrams for (a) ZIF-8, (b) ZIF-90 and (c) ZIF-65 at ambient pressure and (d) ZIF-8, (e) ZIF-90 and (f) ZIF-65 in their respective HP forms at 1.47 GPa, 1.95 GPa and 4.77 GPa respectively. Purple shading represents the solvent accessible volume calculated with a probe size diameter of 3.4 Å (kinetic diameter of methanol) using Mercury.[3] Note the increase in size of the channels linking the central nanopore through the 6MR windows on undergoing the transition.

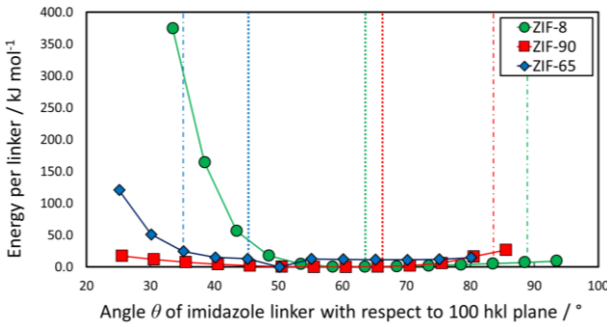

Figure 4: Single point energy calculations showing the energy landscape of the rotation of Im ligands for ZIF-8, ZIF-90 and ZIF-65. Dotted lines denote the crystallographic ambient-pressure phase angle of rotation and dashed lines denote the high-pressure angle of rotation.

of the methyl groups, the rotation of the linker clearly has a definite preference, and in order for the opposite rotation to occur, the energies of adsorption would have to be very large, much larger than what might be expected for adsorption of MeOH which is usually in the order of tens of kJ mol^{-1}.[33]

For both ZIF-90 and ZIF-65, the potential energy landscape determined was relatively flat in comparison to ZIF-8, with only small energy penalties of a few kJ mol^{-1} regardless of the direction of rotation. The difference in behaviour observed for negative linker rotations is attributed to unfavourable CH_3/CH_3 clashing (in the case of ZIF-8), compared to more favourable -CHO or -NO_2 head group interactions in the case of ZIF-90 and ZIF-65, respectively. On compressing ZIF-90, the imidazole rings rotated by approximately +20°. This equated to an energy penalty of just 6.1 kJ mol^{-1}. The corresponding backward rotation equated to 7.5 kJ mol^{-1}. Similarly, for ZIF-65, whilst the highest degree of rotation was -20° at 4.77 GPa, which equated to 25.6 kJ mol^{-1}, the corresponding forward rotation was more favourable at 5.6 kJ mol^{-1}. For all three frameworks, positive rotations are favoured in the absence of any guests. The negative rotations observed in the HP experiments for ZIF-65 therefore indicate a much greater guest-host interaction than for ZIF-90 and ZIF-8.

In order to locate the position of guest MeOH molecules, and to quantify guest-host interactions for ZIF-8, ZIF-65 and ZIF-90, grand canonical Monte Carlo (GCMC) calculations were carried out (for full simulation details see **SI-1**). As GCMC simulations require the frameworks to be rigid, both the ambient pressure (AP) and the highest HP crystallographic structures were used as models in separate GCMC simulations.[15] In this way, the effect of changing the linker orientation on the uptake of methanol into the pores can be directly studied. During the simulations the energies and positions of the methanol molecules were stored, and from this, potential energy histograms constructed (**Fig. 5**). Compared to the AP structures, the guest-host interaction energies for all HP structures

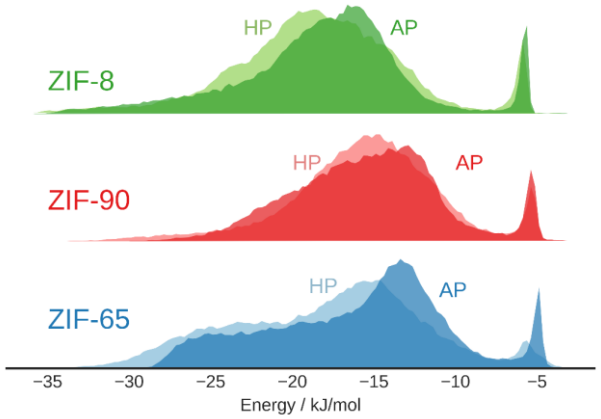

Figure 5: Interaction energy histograms obtained from the highest loading of methanol in ZIFs from GCMC simulations. With ZIF-65, ZIF-90 and ZIF-8 in blue, red and green, respectively. AP (dark) and HP (light) refer to the ambient and high-pressure structures, respectively.

decreased, that is, became more favourable. The driving force for HP phases, for all systems studied, is therefore to maximise the interaction between the framework and the adsorbate – something that was observed before for CH_4 in ZIF-8.[16]

To understand the effect that the guest-host interactions have on the direction of rotation, GCMC simulations were also undertaken on hypothetical structures of ZIF-90 and ZIF-65 where the linkers were rotated by the same degree but in the opposite direction to their HP experimental structures. For example, in ZIF-65-HP, the linkers rotate by -20° compared to the AP phase, so the linkers in the hypothetical structure (named ZIF-65-HYPO) were rotated by +20°. Likewise, the ICA linkers in ZIF-90-HP rotate by + 25°, so the linkers in ZIF-90-HYPO were rotated by -25°. **Fig. 6** shows the resulting methanol – framework interaction energy mapped onto surfaces. The colour of the surface signifies the strength of the interaction. In both ZIF-90-HYPO and ZIF-65-HYPO, the interaction energy between methanol and the framework increases (i.e. becomes less favourable) compared to the experimentally observed structures a strong indication that the guest-framework energies dictate the direction of ligand rotation. See SI-4 for more information on the interaction energies.

Analysing the position of the methanol molecules in the pores sheds light on the differences of packing within the structures, and why each HP structure was preferred over their hypothetical counterpart. For ZIF65-HP (**Fig. 6a**) the most favourable interaction for methanol with the framework (-40 to -30 kJ mol^{-1}) was located just above the four-membered window, interacting strongly with the four overlapping NO_2 groups. The second strongest sites (-30 to -20 kJ mol^{-1}), are found percolating through the structure connecting adjacent pores through the 6MR. The third strongest site (-20 to -10 kJ mol^{-1}), can be found in the pore, as well as in the 6MR window, however these molecules have less favourable orientations to the second site. The final site (-10 to 0 kJ mol^{-1}), was found in the centre of the pore, accounting for the low interaction energy these methanol molecules experience with ZIF-65.

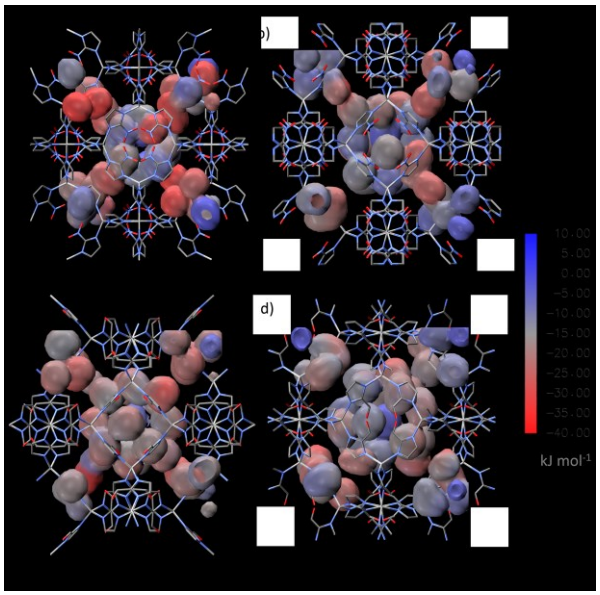

Figure 6: Framework-methanol interaction energy surfaces for (a) ZIF-65-HP, (b) ZIF-65-HYPO, (b) ZIF-90-HP and (d) ZIF-90-HYPO. The scale on the surface represents the interaction energy with blue = 10 kJ mol^{-1} and red = -40 kJ mol^{-1}. Hydrogen atoms are omitted for clarity.

For ZIF-65-HYPO (**Fig. 6b**), there were no methanol –framework interactions below -30 kJ mol^{-1}, most likely due to the orientation of the framework which is now in a gate-opened structure. With the 4MR window open, this orientation does not allow good contact with methanol. The resulting most favourable sites having energies in the order of -30 to -20 kJ mol^{-1}. These sites, like in ZIF-65-HP, sit in the 6MR window thereby connecting the pores throughout the crystal lattice, but with less favourable interaction energies (by ca. 5 kJ mol^{-1}) than in ZIF-65-HP. The second site, blue (-20 to -10 kJ mol^{-1}), was also present in the 6MR window and in the central pore, but the mean interaction energy is again around ~5 kJ mol^{-1} less than ZIF-65-HP. The weakest binding site in ZIF-65-HYPO (-10 to 0 kJ mol^{-1}), occupied the centre of the pore, and the density was much higher than in ZIF-65-HP, which again illustrates that the structure of ZIF-65-HYPO is in a less favourable orientation for the uptake of methanol than ZIF-65-HP. In the case of ZIF-90, the hypothetical phase ZIF-90-HYPO also produced less favourable interaction energies with methanol than ZIF-90-HP. However, the interaction energies are much closer (~1 kJ mol^{-1} difference) compared to ZIF-65, where the offset between each phase is ~3 kJ mol^{-1}.

It is evident that the lowest energy sites (~-30 to -20 kJ mol^{-1}) dictate the orientation of the linkers in the frameworks. These sites percolate from one pore to another through the 6MR windows and it is therefore clear that increasing the limiting pore diameters of these windows is important for adsorption of methanol through the extended pore network. **Fig. 7** and **Table 3** illustrate how for ZIF-90-HP and ZIF-65-HP the diameter of the 6MR windows is larger than for their rotated counterpart structures and ZIF-65-HYPO. For ZIF-65, the highly polar -NO_2 4MR window can form very strong interactions with methanol, which it could not do if it formed a "gate opened" structure like ZIF-8 or ZIF-90, in addition to creating larger channels for the methanol to percolate through the structure.

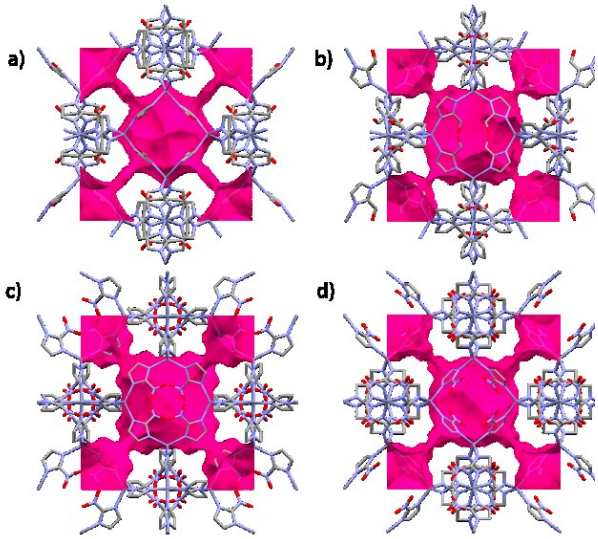

Figure 7: (a) ZIF-90-HP, (b) ZIF-90-HYPO, (c) ZIF-65-HP, (d) ZIF-65-HYPO. All viewed down the 100 direction. Purple shading represents the solvent accessible volume calculated with a probe size diameter of 3.4 Å (kinetic diameter of methanol) using Mercury.[3] Note in (b) and (d) the smaller channels in the six membered ring windows.

Table 3: Table of limiting pore diameters and θ angles of both HP and HYPO phases of ZIF-90 and ZIF-65.

Framework	*θ / °*	*4MR window diameter / Å*	*6MR window diameter/ Å*
ZIF-90-HP	84	2.4	3.6
ZIF-90-HYPO	34	0.0	3.2
ZIF-65-HP	30	0.4	3.8
ZIF-65-HYPO	70	2.0	3.6

In summary, we have demonstrated that the functionality of the imidazole ring dictates the swing effect behaviour of sod ZIFs. By using an alcohol as the hydrostatic medium and by using groups of increasing polarity on the framework in our high pressure X-ray diffraction experiments, we have demonstrated control over the degree of rotation and thus the critical window diameters. We showed that ZIF-90 undergoes a phase transition to a 'gate open' HP phase, however the degree of rotation of the Im linker is less than that of ZIF-8. In addition, it was demonstrated that ZIF-65 undergoes a transition to a more 'gate-closed' structure upon applying high-

pressure. By carrying out DFT simulations of the framework response to ligand rotation, combined with GCMC simulations in the presence of methanol on the HP structures of ZIF-65, ZIF-90 and ZIF-8, and their hypothetical counterparts where the direction of linker rotation is reversed, the guest-host interactions and framework rotation interactions have been deconvoluted. We have demonstrated the importance of guest-framework interactions in the swing-effect mechanism, and it is these interactions which dictate, for SOD topology ZIFs, the direction of the ligand swing. This study opens up the possibilities for exploring these swing-effect frameworks with respect to gas mixtures. Such studies will be invaluable in understanding the competition of guest uptake and how this affects the swing effect mechanism. By exploiting the control over guest – framework interactions, we can work towards creating bespoke molecular sieves.

ASSOCIATED CONTENT

Supporting Information

All computational and experimental methods can be found in the Supporting Information. This material is available free of charge via the Internet at http://pubs.acs.org.
Synthesis and methods for: high-pressure crystallography, DFT geometry optimization, DFT single point energy calculations, grand canonical Monte Carlo simulations; Crystallographic data of ZIF-90 and ZIF-65 at pressure; ZIF-65 geometry changes at pressure; Density functional theory calculations of linker rotations; Grand canonical Monte Carlo simulations of hypothetical ZIF phases.

AUTHOR INFORMATION

Corresponding Author

*c.l.hobday@bath.ac.uk

Present Addresses

† Centre for Advanced Separations Engineering
Department of Chemical Engineering
University of Bath
Claverton Down
Bath BA2 7AY
United Kingdom

Author Contributions

The manuscript was written through contributions of all authors. All authors have given approval to the final version of the manuscript.

Notes

The authors declare no competing financial interest.

ACKNOWLEDGMENT

CLH thanks the EPSRC and University of Edinburgh for a studentship. TDB thanks the Royal Society for funding and for their support. C.A.M. acknowledges the UK Car-Parrinello consortium (EP/P022790/1) for access to the high performance computing resource ARCHER, as managed by the Edinburgh Parallel Computing Service.

REFERENCES

(1) Moggach, S. A.; Bennett, T. D.; Cheetham, A. K. Angew. Chem. Int. Edit. 2009, 48, 7087.
(2) Ryder, M. R.; Civalleri, B.; Bennett, T. D.; Henke, S.; Rudic, S.; Cinque, G.; Fernandez-Alonso, F.; Tan, J. C. Phys. Rev. Lett. 2014, 113.
(3) Macrae, C. F.; Bruno, I. J.; Chisholm, J. A.; Edgington, P. R.; McCabe, P.; Pidcock, E.; Rodriguez-Monge, L.; Taylor, R.; van de Streek, J.; Wood, P. A. J. Appl. Cryst. 2008, 41, 466.
(4) Park, K. S.; Ni, Z.; Cote, A. P.; Choi, J. Y.; Huang, R. D.; Uribe-Romo, F. J.; Chae, H. K.; O'Keeffe, M.; Yaghi, O. M. Proc. Natl. Acad. Sci. U.S.A. 2006, 103, 10186.
(5) Eum, K.; Jayachandrababu, K. C.; Rashidi, F.; Zhang, K.; Leisen, J.; Graham, S.; Lively, R. P.; Chance, R. R.; Sholl, D. S.; Jones, C. W.; Nair, S. J. Am. Chem. Soc. 2015, 137, 4191.
(6) Yen, C. I.; Liu, S. M.; Lo, W. S.; Wu, J. W.; Liu, Y. H.; Chein, R. J.; Yang, R. Q.; Wu, K. C. W.; Hwu, J. R.; Ma, N. H.; Shieh, F. K. Chem-Eur. J. 2016, 22, 2925.
(7) Huang, A. S.; Liu, Q.; Wang, N. Y.; Caro, J. Micropor. Mesopor. Mat. 2014, 192, 18.
(8) Wharmby, M. T.; Henke, S.; Bennett, T. D.; Bajpe, S. R.; Schwedler, I.; Thompson, S. P.; Gozzo, F.; Simoncic, P.; Mellot-Draznieks, C.; Tao, H. Z.; Yue, Y. Z.; Cheetham, A. K. Angew. Chem. Int. Edit. 2015, 54, 6447.
(9) Bennett, T. D.; Sotelo, J.; Tan, J. C.; Moggach, S. A. CrystEngComm 2015, 17, 286.
(10) Bux, H.; Chmelik, C.; van Baten, J. M.; Krishna, R.; Caro, J. Adv. Mater. 2010, 22, 4741.
(11) Kwon, H. T.; Jeong, H. K. Chem. Commun. 2013, 49, 3854.
(12) Pan, Y. C.; Li, T.; Lestari, G.; Lai, Z. P. J Membrane Sci 2012, 390, 93.
(13) Kwon, H. T.; Jeong, H. K. J. Am. Chem. Soc. 2013, 135, 10763.
(14) Bux, H.; Liang, F. Y.; Li, Y. S.; Cravillon, J.; Wiebcke, M.; Caro, J. J. Am. Chem. Soc. 2009, 131, 16000.
(15) Fairen-Jimenez, D.; Moggach, S. A.; Wharmby, M. T.; Wright, P. A.; Parsons, S.; Duren, T. J. Am. Chem. Soc. 2011, 133, 8900.
(16) Fairen-Jimenez, D.; Galvelis, R.; Torrisi, A.; Gellan, A. D.; Wharmby, M. T.; Wright, P. A.; Mellot-Draznieks, C.; Duren, T. Dalton Trans. 2012, 41, 10752.
(17) Zhang, C.; Gee, J. A.; Sholl, D. S.; Lively, R. P. J. Phys. Chem. C 2014, 118, 20727.
(18) Tan, N. Y.; Ruggiero, M. T.; Orellana-Tavra, C.; Tian, T.; Bond, A. D.; Korter, T. M.; Fairen-Jimenez, D.; Zeitler, J. A. Chem. Commun. 2015, 51, 16037.
(19) Im, J.; Yim, N.; Kim, J.; Vogt, T.; Lee, Y. J. Am. Chem. Soc. 2016, 138, 11477.
(20) Huang, A. S.; Caro, J. Angew. Chem. Int. Edit. 2011, 50, 4979.
(21) Morris, W.; Doonan, C. J.; Furukawa, H.; Banerjee, R.; Yaghi, O. M. J. Am. Chem. Soc. 2008, 130, 12626.
(22) Banerjee, R.; Phan, A.; Wang, B.; Knobler, C.; Furukawa, H.; O'Keeffe, M.; Yaghi, O. M. Science 2008, 319, 939.
(23) Moggach, S. A.; Allan, D. R.; Parsons, S.; Warren, J. E. J. Appl. Cryst. 2008, 41, 249.
(24) Piermarini, G. J.; Block, S.; Barnett, J. D.; Forman, R. A. J. Appl. Phys. 1975, 46, 2774.
(25) Forman, R. A.; Block, S.; Barnett, J. D.; Piermarini, G. Science 1972, 176, 284.
(26) Spek, A. L. J. Appl. Cryst. 2003, 36, 7.
(27) Graham, A. J.; Allan, D. R.; Muszkiewicz, A.; Morrison, C. A.; Moggach, S. A. Angew. Chem. Int. Edit. 2011, 50, 11138.
(28) Ortiz, A. U.; Boutin, A.; Fuchs, A. H.; Coudert, F. X. J. Phys. Chem. Lett. 2013, 4, 1861.
(29) Cao, S.; Bennett, T. D.; Keen, D. A.; Goodwin, A. L.; Cheetham, A. K. Chem. Commun. 2012, 48, 7805.
(30) Graham, A. J.; Tan, J. C.; Allan, D. R.; Moggach, S. A. Chem. Commun. 2012, 48, 1535.
(31) Daszkiewicz, M. CrystEngComm 2013, 15, 10427.
(32) Wozniak, K.; He, H. Y.; Klinowski, J.; Jones, W.; Grech, E. J. Phys. Chem. 1994, 98, 13755.
(33) de Lange, M. F.; van Velzen, B. L.; Ottevanger, C. P.; Verouden, K. J. F. M.; Lin, L. C.; Vlugt, T. J. H.; Gascon, J.; Kapteijn, F. Langmuir 2015, 31, 12783.

(Word Style "TF_References_Section"). References are placed at the end of the manuscript. Authors are responsible for the accuracy and completeness of all references. Examples of the recommended formats for the various reference types can be found at http://pubs.acs.org/page/4authors/index.html. Detailed information on reference style can be found in The ACS Style Guide, available from Oxford Press.

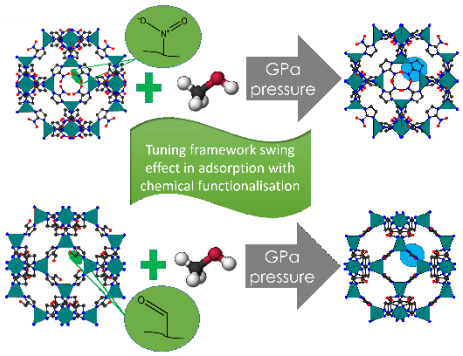
GPa
pressure
Tuning framework swing
effect in adsorption with
chemical functionalisation
GPa
pressure